J|A|C|S
ARTICLES

Published on Web 12/04/2008

Complete Mechanism of σ^* Intramolecular Aromatic Hydroxylation through O_2 Activation by a Macrocyclic Dicopper(I) Complex

Albert Poater,*,† Xavi Ribas,*,‡ Antoni Llobet,§ Luigi Cavallo,† and Miquel Solà*,‡

Modeling Laboratory for Nanostructures and Catalysis (MoLNaC), Dipartimento di Chimica, Università degli Studi di Salerno, via Ponte don Melillo, Fisciano (SA), 84084, Italy, Departament de Química and Institut de Química Computacional, Universitat de Girona, Campus de Montilivi, E-17071, Girona, Catalonia, Spain, and Departament de Química, Universitat Autònoma de Barcelona, Cerdanyola del Vallès, E-08193 Barcelona, Spain and Institute of Chemical Research of Catalonia (ICIQ), Av. Països Catalans 16, E-43007 Tarragona, Spain

Received March 14, 2008; E-mail: albert.poater@udg.edu; xavi.ribas@udg.edu; miquel.sola@udg.edu

Abstract: The present study reports the first example of a complete and detailed mechanism of intramolecular aromatic hydroxylation through O_2 activation by a hexaazamacrocyclic dicoppper(I) complex, $[Cu^I_2(H3m)]^{2+}$. The reactivity of this complex has been previously studied experimentally, although only the characterization of the final μ-phenoxo-μ-hydroxo $[Cu^{II}_2(H3m\text{-}O)(\mu\text{-}OH)]^{2+}$ product was possible. In the present theoretical study, we unravel the reaction pathway for the overall intramolecular aromatic hydroxylation, that is, from the initial reaction of O_2 with the dicopper(I) species to the final $[Cu^{II}_2(H3m\text{-}O)(\mu\text{-}OH)]^{2+}$ product using the B3LYP method. Our results indicate that a Cu^ICu^{II}-superoxo species is formed first, then the interaction of the O_2 moiety with the second Cu^I center leads to a μ-η^2:η^2-peroxo-Cu^{II}_2 intermediate. This latter species is found to be close in energy with the isomeric bis(μ-oxo) species. The relative stability of these two isomers depends on the method of calculation, and therefore, it has not been possible to reach a definite conclusion about the nature of the active species in this reaction mechanism. Notwithstanding, our B3LYP calculations indicate that it is the μ-η^2:η^2-peroxo species that evolves via an electrophilic σ^* attack involving a concerted peroxide O−O bond cleavage and C−O bond formation to a Wheland-type intermediate. The reaction follows with a proton release assisted by the presence of a second aromatic ring yielding a μ-hydroxo-μ-oxo intermediate species, which, in the final stage of the reaction, rearranges to the product. The proton transfer path points out the possibility to design new systems with improved reactivity by properly placing a second aromatic ring to assist the deprotonation step. The lack of high energy barriers and deep energy wells explains the difficulty to trap intermediates experimentally.

Introduction

In addition to the relevant fields of environmental[1] and medicinal chemistry,[2] and to industrial applications,[3] the binding and activation of dioxygen through multiple metal centers play an important role in the catalytic cycle of many metalloenzymes.[4] Hemocyanin, tyrosinase, and catechol oxidases[5] are prototypical cases of proteins containing dinuclear copper active sites capable of transporting or activating O_2. Recently, Matoba et al. reported a crystallographic study on tyrosinase showing a remarkably flexible dicopper binding site where the Cu···Cu distance undergoes large changes along the catalytic cycle, in order to accommodate the bridging molecule.[6] These proteins inspired the work of many research groups, which have focused their investigation on designing biomimetic models with a tunable prearrangement of two metal centers.[5] Understanding the interaction of molecular O_2 with bioinspired dinuclear Cu^I complexes is one of the key issues,[7] and a variety of structural

† Università degli Studi di Salerno.
‡ Universitat de Girona.
§ Universitat Autònoma de Barcelona and ICIQ.

(1) Duran, N.; Esposito, E. *Appl. Catal., B* **2000**, *28*, 83–99.
(2) da Silva, G. F. Z.; Tay, W. M.; Ming, L.-J. *J. Biol. Chem.* **2005**, *280*, 16601–16609.
(3) (a) Tkatchouk, E.; Fomina, L.; Rumsh, L.; Fomine, S. *Macromolecules* **2003**, *36*, 5607–5612. (b) Limberg, C. *Angew. Chem., Int. Ed.* **2003**, *42*, 5932–5954.
(4) (a) Karlin, K. D.; Gultneh, Y. *Prog. Inorg. Chem.* **1987**, *35*, 219–327. (b) Sorrell, T. N. *Tetrahedron* **1989**, *45*, 3–68. (c) Karlin, K. D.; Tyeklar, Z. *Adv. Inorg. Biochem.* **1994**, *9*, 123–172. (d) Solomon, E. I.; Lowery, M. D. *Science* **1993**, *259*, 1575–1581. (e) Que, L., Jr.; Tolman, W. B. *Angew. Chem., Int. Ed.* **2002**, *41*, 1114–1137. (f) Holland, P. L.; Tolman, W. B. *Coord. Chem. Rev.* **1999**, *192*, 855–869.
(5) (a) Solomon, E. I.; Sundaram, U. M.; Machonkin, T. E. *Chem. Rev.* **1996**, *96*, 2563–2606. (b) Mirica, L. M.; Ottenwaelder, X.; Stack, T. D. P. *Chem. Rev.* **2004**, *104*, 1013–1045. (c) Solomon, E. I.; Chen, P.; Metz, M.; Lee, S.-K.; Palmer, A. E. *Angew. Chem., Int. Ed.* **2001**, *40*, 4570–4590. (d) Karlin, K. D.; Kaderli, S.; Zuberbühler, A. D. *Acc. Chem. Res.* **1997**, *30*, 139–147. (e) Decker, H.; Dillinger, R.; Tuczek, F. *Angew, Chem. Int. Ed.* **2000**, *39*, 1591–1595. (f) Lind, T.; Siegbahn, P. E. M.; Crabtree, R. H. *J. Am. Chem. Soc.* **1999**, *103*, 1193–1202. (g) Decker, H.; Schweikardt, T.; Tuczek, F. *Angew. Chem., Int. Ed.* **2006**, *45*, 4546–4550. (h) Siegbahn, P. E. M. *J. Biol. Inorg. Chem.* **2003**, *8*, 567–576. (i) Lewis, E. A.; Tolman, W. B. *Chem. Rev.* **2004**, *114*, 1047–1076.
(6) Matoba, Y.; Kumagai, T.; Yamamoto, A.; Yoshitsu, H.; Sugiyama, M. *J. Biol. Chem.* **2006**, *281*, 8981–8990.

 10.1021/ja801913b CCC: $40.75

motifs for the binding of O_2 have been reported.[8] Experimentally, side-on μ-η^2:η^2-peroxo and bis(μ-oxo) isomeric $Cu_2O_2^{2+}$ cores have been unequivocally characterized in several systems. The crystal structure of a μ-η^2:η^2-peroxo-Cu^{II}_2 species was first described by Kitajima et al. in 1992,[9] while the bis(μ-oxo)-Cu^{III}_2 isomer was first described by Mahapatra et al. in 1995.[10] The interconversion between both isomers is facile and their relative stability can be tuned by the electronic and steric properties of the ligands, and even by using different solvents or counteranions.[11] Both geometries for the $Cu_2O_2^{2+}$ cores have been proposed to be the active species in the aromatic hydroxylation process. However, even carefully designed experiments are often unable to clearly characterize all the intermediates involved in this reaction. Therefore, the nature of the active species in this reaction is still a matter of discussion.[12]

Tyrosinase biomimetic model systems that selectively lead to aromatic hydroxylation products[13] are more abundant than solubleMethane Monooxygenase (sMMO) models that yield stable aliphatic hydroxylation compounds.[14] Theoretically, the situation is reversed and relevant theoretical contributions have shed light on the reaction mechanism for the conversion of methane to methanol in sMMO.[15] It is worth noting here that, recently, Holthausen and co-workers[16] have thoroughly analyzed part of the mechanism of an intramolecular aliphatic hydroxylation process.

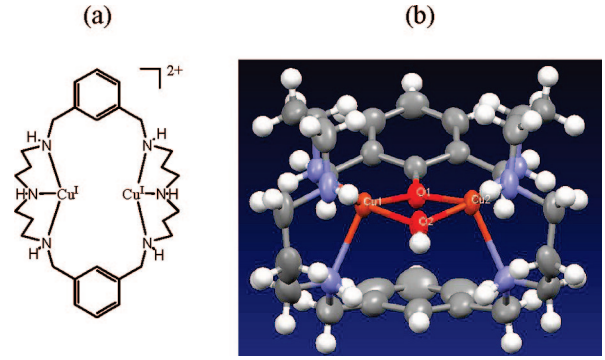

Figure 1. (a) Schematic representation of $[Cu^I_2(H3m)]^{2+}$ (**a**). (b) X-ray structure of μ-phenoxo-μ-hydroxo product $[Cu^{II}_2(H3m\text{-}O)(\mu\text{-}OH)]^{2+}$ (**l**).

On the other hand, beside a recent theoretical study focused only on the O-insertion step of the reaction pathway for the aromatic *ortho*-hydroxylation of phenoxide in a model system,[17] a detailed and complete quantum-mechanical description of the mechanism of the intramolecular aromatic hydroxylation, from the initial Cu^I species to the hydroxylated product, is still missing. In the present study we try to fulfill this gap. To this end, we focused our attention on the hexaazamacrocyclic dinuclear Cu^I complex $[Cu^I_2(H3m)](PF_6)_2$ (**a**) (Figure 1a).[8c] This complex reacts with O_2 in acetonitrile solvent to yield the μ-phenoxo-μ-hydroxo product $[Cu^{II}_2(H3m\text{-}O)(\mu\text{-}OH)](PF_6)_2$ (**l**) (Figure 1b), through an intramolecular aromatic hydroxylation reaction (removal of metal ions affords the monohydroxylated ligand H3m-OH).[8d] Compound **l** was characterized by X-ray spectroscopy but no intermediates in the reaction pathway from **a** + O_2 to **l** were detected,[8d] despite carefully designed stopped-flow UV−vis experiments that were performed. For this system, we analyze in detail the whole reaction pathway, from the initial binding of O_2 to complex **a** to the final product **l** by means of density functional theory (DFT) calculations.

Theoretical Methods

All geometry optimizations, with no symmetry constraints, have been performed with the Gaussian03 package,[18] using the B3LYP functional[19] and the standard 6−31G(d) basis set.[20] The geometries obtained at the B3LYP/6−31G(d) level were used to perform single-point energy calculations with a larger basis set, the 6−311G(d,p) basis set,[21] and the same functional (B3LYP/6−311G(d,p)//B3LYP/6−31G(d)). Intrinsic reaction pathways were calculated to confirm that the transition states located connected the expected minima. Analytical Hessians were computed to determine the nature of all the stationary points we located, and to calculate zero-point energies (ZPEs) and thermodynamic properties at 298 K.

(7) Lewis, A. E.; Tolman, W. B. *Chem. Rev.* **2004**, *104*, 1047–1076.
(8) (a) Lewin, J. L.; Heppner, D. E.; Cramer, C. J. *J. Biol. Inorg. Chem.* **2007**, *12*, 1221–1234. (b) Cramer, C. J.; Wloch, M.; Piecuch, P.; Puzzarini, C.; Gagliardi, L. *J. Phys. Chem. A* **2006**, *110*, 1991–2004; Erratum ibid. **2007**, *111*, 4817. (c) Rode, M. F.; Werner, H.-J. *Theor. Chem. Acc.* **2005**, *114*, 309–317. (d) Costas, M.; Ribas, X.; Poater, A.; López-Valbuena, J. M.; Xifra, R.; Company, A.; Duran, M.; Solà, M.; Llobet, A.; Corbella, M.; Usón, M. A.; Mahía, J.; Solans, X.; Shan, X.; Benet-Buchholz, J. *Inorg. Chem.* **2006**, *45*, 3569–3581. (e) Menif, R.; Martell, A. E.; Squattrito, P. J.; Clearfield, A. *Inorg. Chem.* **1990**, *29*, 4723–4729. (f) Malmqvist, P. A.; Pierloot, K.; Shahi, A. R. M.; Cramer, C. J.; Gagliardi, L. *J. Chem. Phys.* **2008**, *128*, 204109–201110.
(9) Kitajima, N.; Fujisawa, K.; Fujimoto, C.; Morooka, Y.; Hashimoto, S.; Kitagawa, T.; Torinmi, K.; Tatsumi, K.; Nakamura, A. *J. Am. Chem. Soc.* **1992**, *114*, 1277–1291.
(10) Mahapatra, S.; Halfen, J. A.; Wilinson, E. C.; Pan, G.; Cramer, C. J., Jr.; Tolman, W. B. *J. Am. Chem. Soc.* **1995**, *117*, 8865–8866.
(11) (a) Halfen, J. A.; Mahapatra, S.; Wilkinson, E. C.; Kaderli, S.; Young, V. G., Jr.; Que, L., Jr.; Zuberbühler, A. D.; Tolman, W. B. *Science* **1996**, *271*, 1397–1400. (b) Mahapatra, S.; Halfen, J. A.; Tolman, W. B. *J. Am. Chem. Soc.* **1996**, *118*, 11575–11586. (c) Osako, T.; Tachi, Y.; Taki, M.; Fukuzumi, S.; Itoh, S. *Inorg. Chem.* **2001**, *40*, 6604–6609. (d) Hatcher, L. Q.; Vance, M. A.; Narducci Sarjeant, A. A.; Solomon, E. I.; Karlin, K. D. *Inorg. Chem.* **2006**, *45*, 3004–3013.
(12) (a) Mirica, L. M.; Vance, M.; Jackson-Rudd, D.; Hedman, B.; Hodgson, K. O.; Solomon, E. I.; Stack, T. D. P. *Science* **2005**, *308*, 1890–1892. (b) Company, A.; Palavicini, S.; Garcia-Bosch, I.; Mas-Ballesté, R.; Que, L., Jr.; Rybak-Akimova, E. V.; Casella, L.; Ribas, X.; Costas, M. *Chem.−Eur. J.* **2008**, *14*, 3535–3538.
(13) (a) Palavicini, S.; Granata, A.; Monzani, E.; Casella, L. *J. Am. Chem. Soc.* **2005**, *127*, 18031–18036. (b) Battaini, G.; Monzani, E.; Perotti, A.; Para, C.; Casella, L.; Santagostini, L.; Gullotti, M.; Dillinger, R.; Näther, C.; Tuczek, F. *J. Am. Chem. Soc.* **2003**, *125*, 4185–4198. (c) Santagostini, L.; Gullotti, M.; Monzani, E.; Casella, L.; Dillinger, R.; Tuczek, F. *Chem.−Eur. J.* **2000**, *6*, 519–522. (d) Karlin, K. D.; Nasir, M. S.; Cohen, B. I.; Cruse, R. W.; Kaderli, S.; Zuberbühler, A. D. *J. Am. Chem. Soc.* **1994**, *116*, 1324–1336. (e) Mahapatra, S.; Kaderli, S.; Llobet, A.; Neuhold, Y.-M.; Palanche, T.; Halfen, J. A.; Young, V. G., Jr.; Kaden, T. A.; Que, L., Jr.; Zuberbuhler, A. D.; Tolman, W. B. *Inorg. Chem.* **1997**, *36*, 6343–6356. (f) Yamazaki, S.; Itoh, S. *J. Am. Chem. Soc.* **2003**, *125*, 13034–13035. (g) Granata, A.; Monzani, E.; Bubacco, L.; Casella, L. *Chem.−Eur. J.* **2006**, *12*, 2504–2514. (h) De, A.; Mandal, S.; Mukherjee, R. *J. Inorg. Biochem.* **2008**, *102*, 1170–1189.
(14) (a) Itoh, S.; Taki, M.; Nakao, H.; Holland, P. L.; Tolman, W. B.; Que, L., Jr.; Fukuzumi, S. *Angew. Chem. Int. Ed* **2000**, *39*, 398–400. (b) Balasubramanian, R.; Rosenzweig, A. C. *Acc. Chem. Res.* **2007**, *40*, 573–580. (c) Rolff, M.; Tuczek, F. *Angew. Chem., Int. Ed.* **2008**, *47*, 2344–2347.
(15) (a) Yoshizawa, K.; Shiota, Y. *J. Am. Chem. Soc.* **2006**, *128*, 9873–9881. (b) Yoshizawa, K.; Suzuki, A.; Shiota, Y.; Yamabe, T. *Bull. Chem. Soc. Jpn.* **2000**, *73*, 815–827.
(16) Spuhler, P.; Holthausen, M. C. *Angew. Chem., Int. Ed.* **2003**, *42*, 5961–5965.
(17) Naka, N.; Kondo, Y.; Usui, S.; Hashimoto, Y.; Uchiyama, M. *Adv. Synth. Catal.* **2007**, *349*, 595–600.
(18) Frisch, M. J.; et al. Gaussian 03, revision C.02; Gaussian, Inc.: Wallingford, CT, 2004.
(19) (a) Becke, A. D. *J. Chem. Phys.* **1993**, *98*, 5648–5652. (b) Lee, C.; Yang, W.; Parr, R. G. *Phys. Rev. B* **1988**, *37*, 785–789. (c) Stevens, P. J.; Devlin, F. J.; Chabalowski, C. F.; Frisch, M. *J. Phys. Chem.* **1994**, *98*, 11623–11627.
(20) (a) Hehre, W. J.; Ditchfield, R.; Pople, J. A. *J. Chem. Phys.* **1972**, *56*, 2257–2261. (b) Hehre, W. J.; Radom, L.; Schleyer, P. v. R.; Pople, J. A. *Ab Initio Molecular Orbital Theory*; Wiley: New York, 1986.

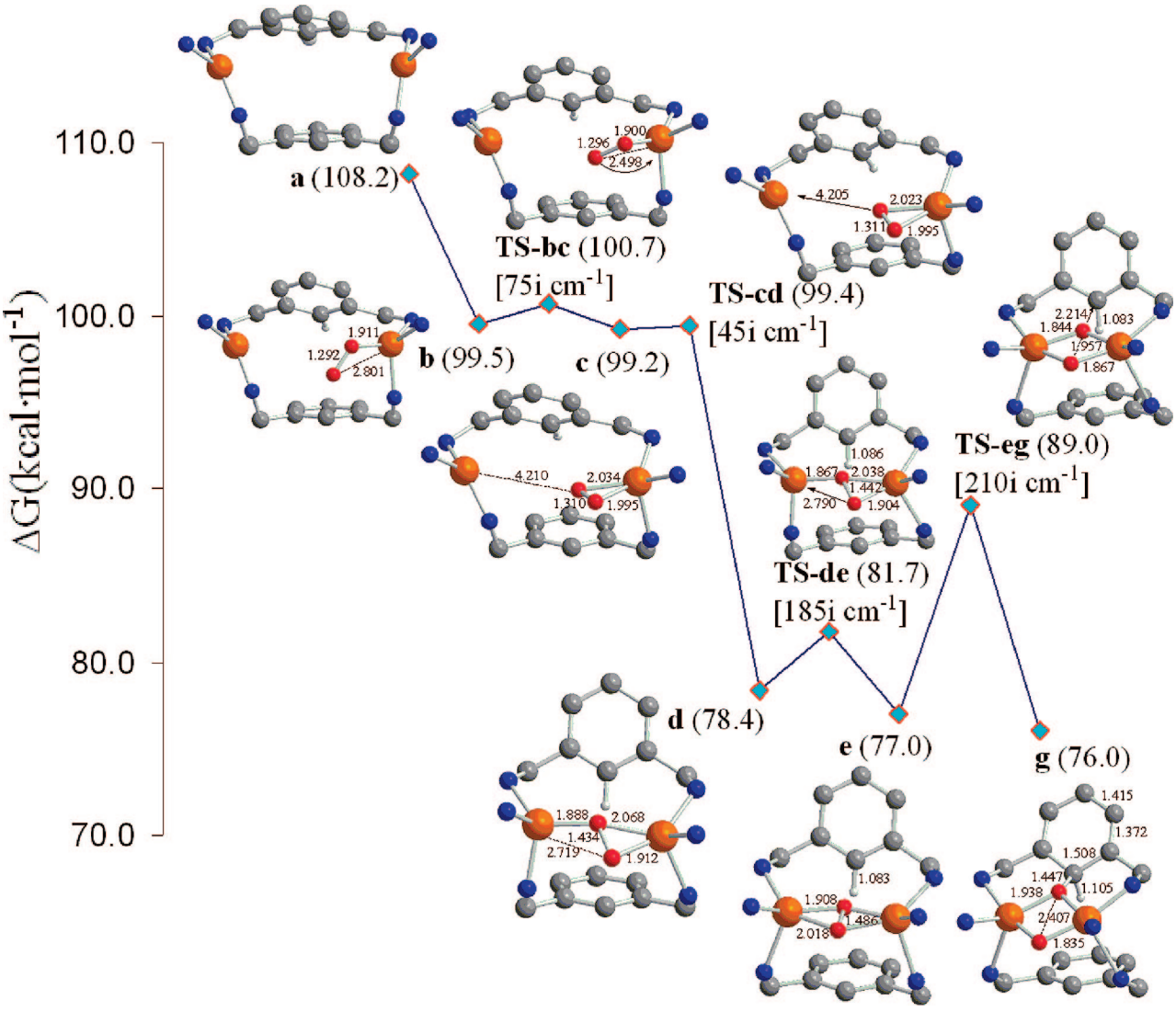

Figure 2. Stationary points along the first half of the reaction pathway of the aromatic hydroxylation mechanism from reactant **a** to intermediate **g** (the second half is shown in Figure 4). For the sake of clarity non-relevant H and C atoms have been omitted. Free energies in solution (CH_3CN as the solvent) relative to Product **I** (see Figure 4) are given in parentheses. The imaginary frequency characterizing the transition state structures is given in brackets. Selected distances are given in Å.

For open-shell states,the geometry optimizations were performed within the broken-symmetry unrestricted methodology, while for the closed-shell singlet states the restricted formalism was used. Theoretical treatment of biradical singlet species requires multiconfigurational or multireference methods due to strong static electron correlation. Unfortunately, these methods can only be applied to relatively small systems because computationally they are extremely demanding. As an alternative, we have used the unrestricted UB3LYP method in broken symmetry (BS, using GUESS = MIX).[22] This method improves the modeling of biradical singlet states at the expense of introducing some spin contamination from higher spin states.[23,24] Although this is not the most appropriate method to treat biradical singlet species, it has been shown that it can be used provided that the overlap between the open-shell orbitals is small (i.e., the unpaired electrons are located in separated atomic centers), which is the case of the systems that show predominant biradical character in this work.[23g] In a previous paper, some of us showed that, for *p*-benzyne, the application of

(21) For Cu, this basis corresponds to the (14s9p5d)/[9s5p3d] Wachters basis set: (a) Wachters, A. J. H. *J. Chem. Phys.* **1970**, *52*, 1033–1036 with the contraction scheme 611111111/51111/311 supplemented with one f polarization function. In the Gaussian 03 implementation of the Cu basis set, the s and p functions come from Wachter's optimization for the Cu atom in its ^{2}S state, while the d functions come from Wachter's optimization for the Cu atom in its ^{2}D state. In a previous work, (b) Güell, M.; Luis, J. M.; Rodríguez-Santiago, L.; Sodupe, M.; Solà, M. *J. Phys. Chem. A* **2008**, submitted for publication), it was reported that the Gaussian 03 internal basis set provides more reasonable results for the relative energies among the different analyzed states than the basis set with the d functions coming from Wachter's optimization for the Cu atom in its ^{2}D state.

(22) Caballol, R.; Castell, O.; Illas, F.; Moreira, I.; d, P. R.; Malrieu, J. P. *J. Phys. Chem. A* **1997**, *101*, 7860–7866.

(23) (a) Winkler, M. *J. Phys. Chem. A* **2005**, *109*, 1240–1246. (b) Lindh, R.; Bernhardsson, A.; Schütz, M. *J. Phys. Chem. A* **1999**, *103*, 9913–9920. (c) Cramer, C. J. *J. Chem. Soc., Perkin Trans. 2* **1999**, 2273–2283. (d) Kikuchi, A.; Ito, H.; Abe, J. *J. Phys. Chem. B* **2005**, *109*, 19448–19453. (e) Borden, W. T. Diradicals. In *The Enciclopedia of Computational Chemistry*; Schleyer, P. v. R., Allinger, N. L., Clark, T., Gasteiger, J., Kollman, P. A., Schaeffer, H. F., III., Eds.; John Wiley & Sons: Chichester, U.K., 1998; pp 708−722. (f) Poater, J.; Bickelhaupt, F. M.; Solà, M. *J. Phys. Chem. A* **2007**, *111*, 5063–5070. (g) Gräfenstein, J.; Kraka, E.; Filatov, M.; Cremer, D. *Int. J. Mol. Sci* **2002**, *3*, 360–394.

(24) Borden, W. T.; Davidson, E. R. *Acc. Chem. Res.* **1996**, *29*, 67–75.

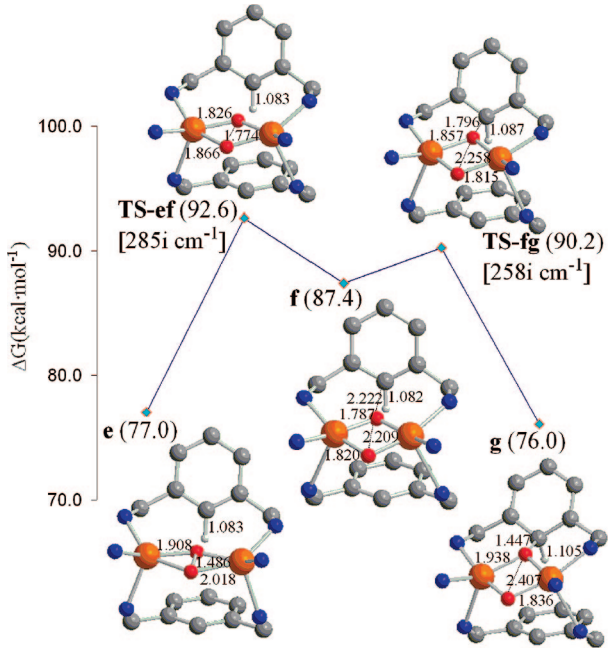

Figure 3. Computed structures for the alternative mechanism that links **e** with **g** via a bis(μ-oxo)-Cu^{III}_2 isomer **f** (distances in Å).

the sum rule[23f] to the energy of the biradical singlet state to remove the spin contamination error does not improve the calculated singlet−triplet energy gap but rather leads to larger errors when compared to the experimental value. For this reason, open-shell singlet energies reported in this work does not contain spin contamination corrections.

Solvent effects including contributions of non electrostatic terms have been estimated in single point calculations on the gas phase optimized structures, based on the polarizable continuous solvation model (PCM) using CH_3CN as a solvent, the same solvent used experimentally. The solvent effect was introduced by the conductor polarizable calculation model (CPCM).[25] The cavity is created via a series of overlapping spheres.

The relative free energies reported in this work include energies computed using the B3LYP/6−311G(d,p)//B3LYP/6−31G(d) method together with solvent effects obtained at the B3LYP/6−31G(d) level and zero-point energies, thermal corrections, and entropy effects calculated at 298 K with the B3LYP/6−31G(d) method.

Finally, in some cases we discuss the change in the local aromaticity of a given ring. As a structure-based measure, we have made use of the harmonic oscillator model of aromaticity (HOMA) index, defined by Kruszewski and Krygowski as:[26]

$$\mathrm{HOMA} = 1 - \frac{\alpha}{n}\sum_{i=1}^{n}(R_{\mathrm{opt}} - R_i)^2 \qquad (1)$$

where n is the number of bonds considered, and α is an empirical constant (for CC bonds $\alpha = 257.7$) fixed to give HOMA = 0 for a model nonaromatic system, and HOMA = 1 for a system with all bonds equal to an optimal value R_{opt}, which is 1.388 Å for CC bonds, assumed to be achieved for fully aromatic systems. R_i stands for a running bond length. We have also used the nucleus independent chemical shift (NICS), proposed by Schleyer and co-workers,[27] as a magnetic index of aromaticity. This is one of the most widely employed indicators of aromaticity. It is defined as the negative value of the absolute shielding computed at a ring center or at some other interesting point of the system. Rings with large negative NICS values are considered aromatic. Among the different NICS indexes, we have used the NICS(1) value, which is considered to better describe the π-electron currents than NICS(0).[28]

Results and Discussion

The starting point of this study was the optimization of complex $[Cu^I_2(H3m)]^{2+}$ (**a**).[29] Crystallographic data on related copper compounds using the same ligand suggest that complex **a** may present many conformations of rather similar energy.[31] The initial conformation to perform the geometry optimization was obtained from the X-ray structure of complex **l** (Figure 1b) by removing the O atoms and attaching the H atom linked to the O2 atom to the aromatic ring (see Figure 1b for the atomic labels). It is worth noting that for all the species we have computed the closed-shell singlet, the biradical singlet, the triplet, and the quintuplet electronic states. Both the quintuplet and the closed-shell singlet states were always found to have much higher energy than the biradical singlet and the triplet states, and thus they are not included in the discussion. On the other hand, the energy difference between the biradical singlet and the triplet states is lower than 5 kcal·mol^{-1} in all cases. In addition, the $\langle S^2\rangle$ values reported in Table S2 of the Supporting Information show that for all the structures in the biradical singlet state $\langle S^2\rangle$ is close to 1 with the exception of intermediate **e** and of transition state **TS-eg** for which $\langle S^2\rangle$ is 0.700 and 0.549, respectively. For all the structures in the triplet state, instead, $\langle S^2\rangle$ is close to 2. These $\langle S^2\rangle$ values correspond to the Slater determinants constructed from Kohn−Sham orbitals as approximate wave functions. Such small biradical singlet−triplet energy gaps and $\langle S^2\rangle$ values are consistent with species having the two spins weakly coupled as a result of a small overlap between the molecular orbitals corresponding to the unpaired electrons.

Binding of O_2 to complex **a** results in the formation of a mixed valence end-on Cu^ICu^{II}-superoxo species **b** with a triplet ground-state through a barrierless process. Species **b** can easily convert into the almost isoenergetic side-on Cu^ICu^{II}-superoxo isomeric species **c**. The barrier for this conversion requires only 1.2 kcal·mol^{-1}. Complex **c** is partially stabilized by the presence of a hydrogen bond between O2 and the H atom of the nearest amine group. Complex **c** evolves to the μ-η^1:η^2-peroxo isomer **d** with an energetic stabilization of 20.8 kcal·mol^{-1}. Conversion from **c** to **d** involves rotation of nearly 180° of the O_2 moiety with respect to the Cu−Cu axis. The Cu1−O1 bond is formed after the overcoming of the low barrier of 3.3 kcal·mol^{-1} yielding the μ-η^2:η^2-peroxo-Cu^{II}_2 isomer **e**. This transformation is accompanied by a change in the multiplicity from triplet to biradical singlet (the energy difference between the triplet and the biradical states is lower than 1 kcal·mol^{-1} due to the large spatial separation between the two unpaired electrons located

(25) (a) Barone, V.; Cossi, M. *J. Phys. Chem. A* **1998**, *102*, 1995–2001. (b) Tomasi, J.; Persico, M. *Chem. Rev.* **1994**, *94*, 2027–2094.
(26) (a) Kruszewski, J.; Krygowski, T. M. *Tetrahedron Lett.* **1972**, 3839–3842. (b) Krygowski, T. M. *J. Chem. Inf. Comp. Sci.* **1993**, *33*, 70–78.
(27) Schleyer, P. v. R.; Maerker, C.; Dransfeld, A.; Jiao, H.; van Eikema Hommes, N. J. R. *J. Am. Chem. Soc.* **1996**, *118*, 6317–6318.
(28) (a) Schleyer, P. v. R.; Manoharan, M.; Wang, Z. X.; Kiran, B.; Jiao, H. J.; Puchta, R.; van Eikema Hommes, N. J. R. *Org. Lett.* **2001**, *3*, 2465–2468. (b) Corminboeuf, C.; Heine, T.; Seifert, G.; Schleyer, P. v. R.; Weber, J. *Phys. Chem. Chem. Phys.* **2004**, *6*, 273–276.
(29) The optimized geometry of **l** is in perfect agreement with the X-ray structure (rmsd = 0.032 Å on distances and 1.4° on angles).[30] See Supporting Information for details.
(30) Poater, A.; Moradell, S.; Pinilla, E.; Poater, J.; Solà, M.; Martínez, M. A.; Llobet, A. *Dalton Trans.* **2006**, 1188–1196.
(31) Company, A.; Jee, J.-E.; Ribas, X.; López-Valbuena, J. M.; Gómez, L.; Corbella, M.; Llobet, A.; Mahía, J.; Benet-Buchholz, J.; Costas, M.; van Eldik, R. *Inorg. Chem.* **2007**, *46*, 9098–9110.

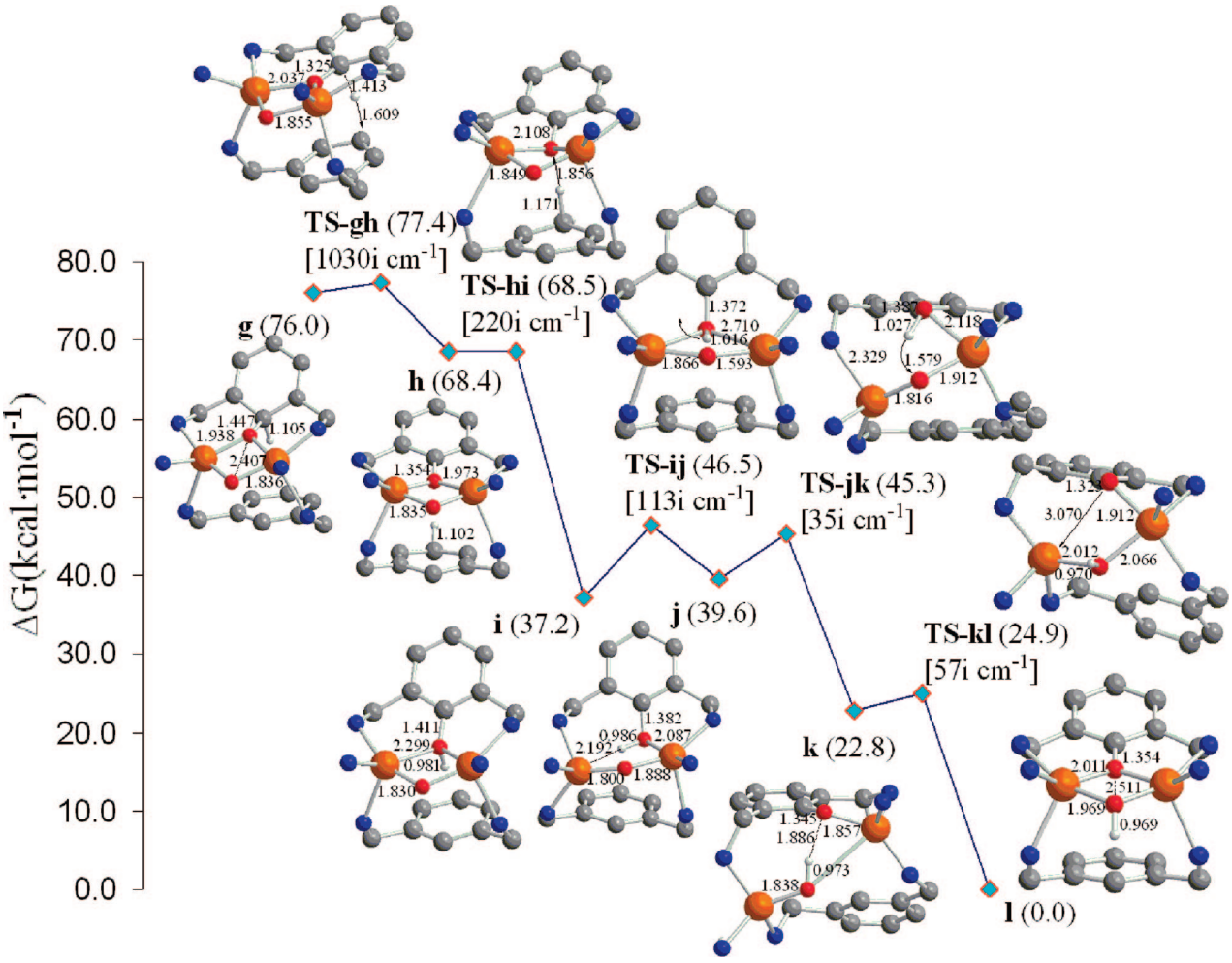

Figure 4. Stationary points along the second half of the reaction pathway of the aromatic hydroxylation mechanism from intermediate **g** to product **l** (the first half is shown in Figure 2). For the sake of clarity nonrelevant H and C atoms have been omitted. Free energies in solution (CH_3CN as the solvent) relative to product **l** are given in parentheses. The imaginary frequency characterizing the transition state structures is given in brackets. Selected distances are given in Å.

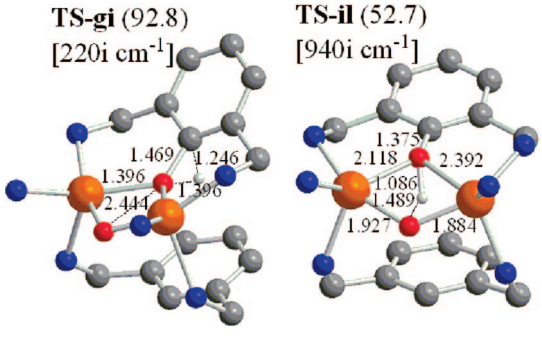

Figure 5. Computed structures for the transition states involved in potential alternative pathways of the σ^* mechanism (energies in kcal·mol^{-1} and distances in Å).

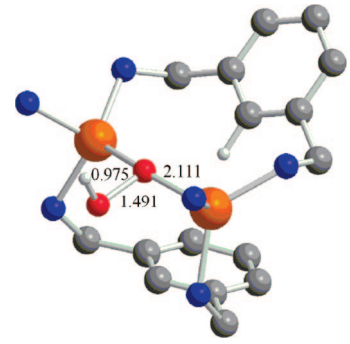

Figure 6. Computed structure for the μ-η^1:η^1-hydroperoxo-Cu^{II}_2 intermediate (distances in Å).

one on each copper atom, as found in similar copper complexes).[32] Interestingly, the optimized complex **e** possesses the two aromatic rings in a perpendicular conformation (Figure 2), providing a perfect scenario for alternative routes (σ^* and π^* attacks) for aromatic hydroxylation (*vide infra*).[5e,12]

Two possible paths from **e** to **g** (C−O bond formation) have been studied. In the former, which is shown in Figure 2, cleavage and consequently elongation of the O−O bond distance in the peroxide **e** results in a direct and concerted attack to the closest C atom of the aromatic ring to form species **g** through a barrier of 12.0 kcal·mol^{-1}. This attack corresponds to the so-

(32) (a) Hong, S.; Huber, S. M.; Gagliardi, L.; Cramer, C. J.; Tolman, W. B. *J. Am. Chem. Soc.* **2007**, *129*, 14190–14192. (b) Cramer, C. J.; Kinal, A.; Wloch, M.; Piecuch, P.; Gagliardi, L. *J. Phys. Chem. A* **2006**, *110*, 11557–11568. (c) Bernardi, F.; Bottoni, A.; Casadio, R.; Fariselli, P.; Rigo, A. *Inorg. Chem.* **1996**, *35*, 5207–5212.

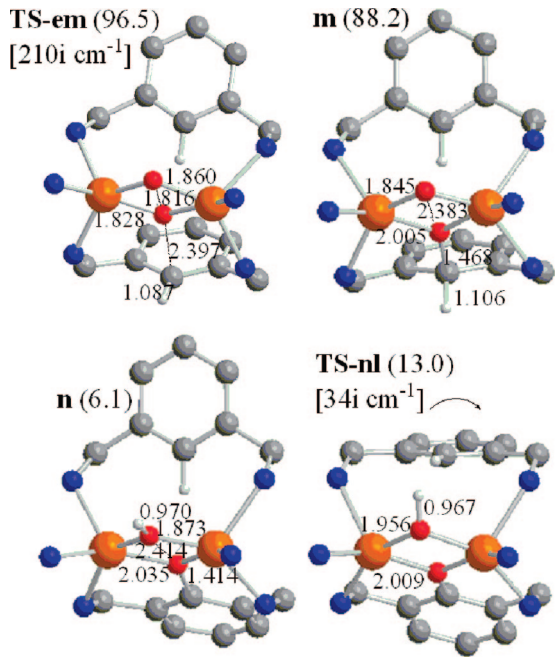

Figure 7. Computed structures for minima and transition states involved in the possible intramolecular electrophilic attack of the $Cu_2O_2^{2+}$ core to the second aromatic ring of the ligand scaffold (energies in kcal·mol^{-1} and distances in Å).

called σ* electrophilic mechanism described for the *ortho*-hydroxylation of phenolates.[5e] In the alternative route (see Figure 3), the μ-η^2:η^2-peroxo-Cu^{II}_2 intermediate **e** evolves first to the closed-shell singlet bis(μ-oxo)-Cu^{III}_2 isomer **f** after surmounting the rather large barrier of 15.6 kcal·mol^{-1}. This bis(μ-oxo) species, which is 10.4 kcal·mol^{-1} higher in energy with respect to the peroxo form **e**, can subsequently be converted into species **g** by attack of the O1 atom to the nearby C atom of the aromatic ring, by passing a small barrier of 2.8 kcal·mol^{-1}. These results indicate that the direct **e** → **g** pathway of Figure 2 is favored with respect to the **e** → **f** → **g** pathway of Figure 3 because of the higher energy barrier required for the **e** → **f** step.

At this point, a digression on the relative stability of the μ-η^2:η^2-peroxo and of the bis(μ-oxo) species **e** and **f** is needed. As reported by Cramer,[8a,b,33] the equilibrium between the two isomers is artificially displaced toward the peroxo species by hybrid functionals such as the B3LYP functional, due to unbalanced correlation corrections, while pure functionals like the BLYP functional provide better relative energies.[8a,b] Indeed, test calculations with the BLYP functional show that the preference for the μ-η^2:η^2-peroxo species **e** is reduced from 10.4 to −4.4 kcal·mol^{-1} when switching from the hybrid B3LYP functional to the pure BLYP functional. However, it is important to remark here that the calculated energy difference between these two species depends on several effects such as the percentage of Hartree−Fock exchange in hybrid functionals, inclusion of solvent effects, and the use of different basis sets.[34] For instance, test calculations with the BLYP functional, without including zero-point energies, thermal corrections, and entropy effects, indicate that the bis-μ-oxo form **f** is favored by 3.1 kcal·mol^{-1} when the smaller 6−31G(d) basis set is used, but less favored by 1.6 kcal·mol^{-1} with the 6−311G(d,p) basis set. In conclusion, although our calculations indicate that the μ-η^2:η^2-peroxo species is the active species in the hydroxylation process studied here, the presence of the bis(μ-oxo) isomer in the reaction pathway can not be totally ruled out. Highly correlated methods should be used to solve this issue, but the size of the systems precludes this possibility. Nevertheless, apart from the equilibrium between the μ-η^2:η^2-peroxo and bis(μ-oxo) isomers, the reliability of B3LYP relative energies has been substantiated by previous studies.[17,35]

After this digression on the relative stability of the μ-η^2:η^2-peroxo and of the bis(μ-oxo) species, we return to the mechanism of aromatic hydroxylation by describing intermediate **g**. Species **g** shows a dearomatization of the ring due to the formation of the C−O bond, with a concomitant change in the hybridization of the attacked carbon atom from sp^2 to sp^3 (see Figure 2). Intermediate **g** is well described as a Wheland arenium species (HOMA and NICS(1) indexes of the attacked aromatic ring change from 0.970 to −0.328 and from −11.64 ppm to 2.10 ppm, respectively, on going from **e** to **g**), which are typically prone to deprotonation and subsequent recovery of the aromaticity.[36] In previous studies on *ortho*-hydroxylation of phenols, the latter species is not found since the alcohol group participates in the stabilization of the dearomatized ring.[17]

Noteworthy, in the next reaction step the aromatic H atom of the activated C−H bond of **g** migrates as a proton to the other aromatic ring (which is kept parallel to the $Cu_2O_2^{2+}$ core from **a** to **g**, see Figure 4) to form compound **h** through a barrier of only 1.4 kcal·mol^{-1}. This proton transfer is favored by the close proximity of the two rings (the distance of the proton to the centroid of the other aromatic ring is <2.6 Å) and by the higher basicity of the unsubstituted aromatic ring compared to the initially attacked ring (consider relative energies of **g** and **h**). In species **h** the attacked ring has recovered the aromaticity and the second ring becomes dearomatized (HOMA and NICS(1) indexes of the aromatic and nonaromatic six-membered rings in **h** are 0.939 and −0.252 and −10.34 ppm and 0.74 ppm, respectively). In the following step, the proton that has been transferred in the **g** → **h** step is now transferred to O1 yielding intermediate **i** by overcoming an almost negligible barrier of 0.1 kcal·mol^{-1}. The direct **g** → **i** transformation requires the overcoming of a barrier of 16.8 kcal·mol^{-1} and, consequently, we have discarded this route (see Figure 5). In compound **i** the aromaticity of both six-membered rings have been recovered, which explains its remarkable stability compared to intermediates **g** and **h**.

The next step involves the cleavage of the Cu1−O1 bond of **i**, with a barrier of 9.3 kcal·mol^{-1}, leading to the hydroxo-(μ-oxo) intermediate **j**. A subsequent transfer of the proton from O1 to O2, through a barrier of only 5.7 kcal·mol^{-1}, leads to species **k**. Rotation of the hydroxyl -O2H group in **k** and reconstruction of the Cu1−O1 bond, with an energetic barrier of 2.1 kcal·mol^{-1}, yields species **l**, the experimental product of the reaction.

Considering the complexity of the multisteps reaction pathway of Figures 2 and 4, we have made extensive tests to check if some of the intermediates could be connected more straightforwardly. However, all the attempts resulted in higher energy

(33) Gherman, B. F.; Cramer, C. J. *Coord. Chem. Rev.* **2008**, doi:10.1016/j.ccr.2007.11.018.
(34) Güell, M.; Luis, J. M.; Solà, M.; Siegbahn, P. E. M. *J. Biol. Inorg. Chem.* **2008**, doi:10.1007/s00775-008-0443-y.
(35) (a) Siegbahn, P. E. M. *J. Biol. Inorg. Chem.* **2003**, *8*, 577–585. (b) Güell, M.; Siegbahn, P. E. M. *J. Biol. Inorg. Chem.* **2007**, *12*, 1251–1264.
(36) Hubig, S. M.; Lindeman, S. V.; Kochi, J. K. *Coord. Chem. Rev.* **2000**, *200−202*, 831–873.

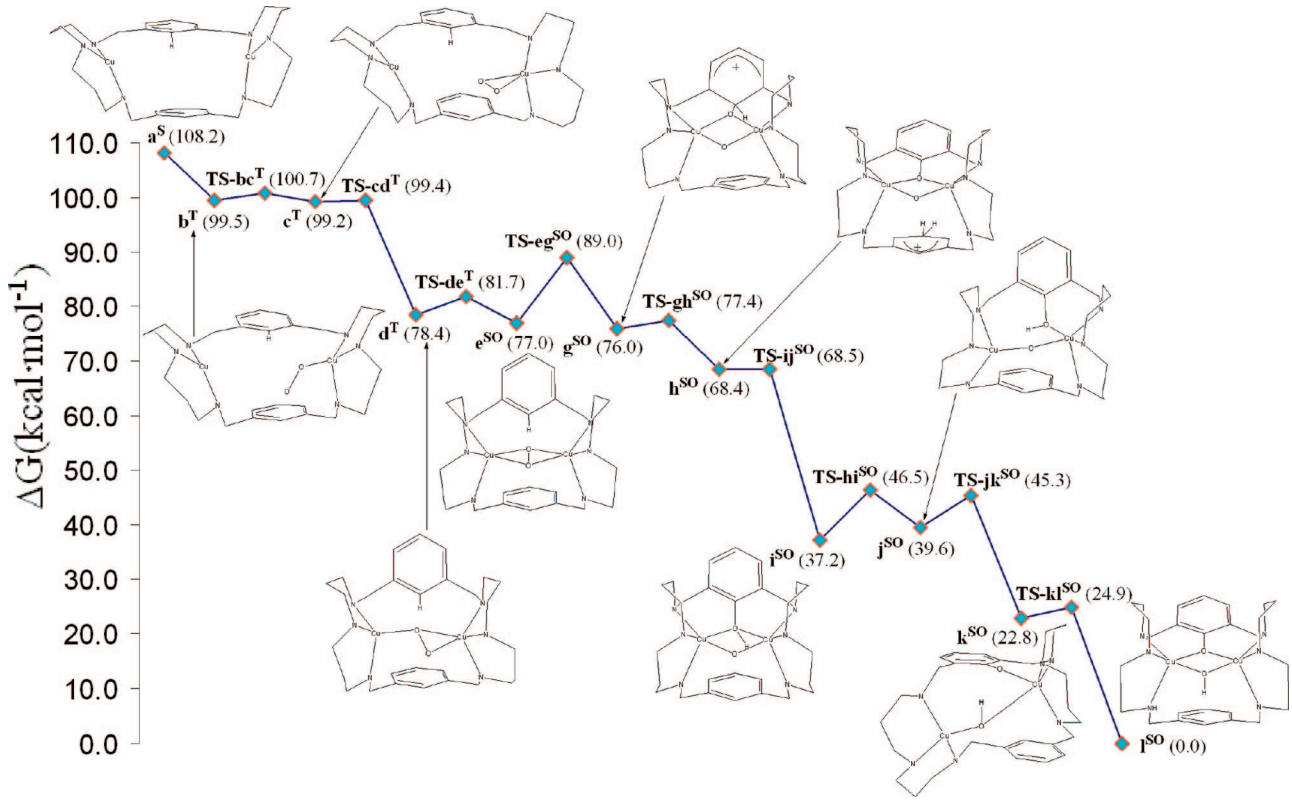

Figure 8. Free energy profile for the calculations of all stationary points located along the reaction path of the aromatic hydroxylation mechanism starting from complex **a** and finishing into the intramolecular aromatic hydroxylation product, **l** (some H atoms omitted for clarity). Free energies relative to product (in kcal·mol^{-1}) in solution are given in parentheses. Superindexes S (closed-shell singlet), SO (open-shell singlet), and T (triplet) refer to the multiplicity of the ground state.

barriers. For instance, beside the direct **g** → **h** step we have discussed previously, we also explored the direct **i** → **l** proton transfer from O1 to O2, but transition state **TS-il** for this direct proton transfer (see Figure 5) is 6.2 kcal·mol^{-1} higher in energy compared to transition state **TS-ij**, and therefore the direct **i** → **l** pathway was discarded in favor of the multisteps **i** → **j** → **k** → **l** pathway. It is worth noting indeed that the latter multistep pathway is analogous to that found in an aliphatic hydroxylation reaction reported by Spuhler and Holthausen.[16]

Lastly, concerning a direct **g** → **l** transformation assisted by solvent molecules, we have performed calculations including an explicit acetonitrile molecule that may assist the extraction of a proton from species **g**. However, all attempts to simulate such an assisted proton transfer pathway failed because there is no space left between the Cu_2O_2 core and the second aromatic ring (distance from O2 to the closest aromatic H is 2.928 Å in **g**) to allow the introduction of an acetonitrile molecule in the channel, which would then assist the proton transfer directly to O2. However, it is worth noting that the energetic balance of extracting the proton from species **g** by an acetonitrile molecule is favorable. Thus, the reaction **g** + acetonitrile → unprotonated **g** + protonated acetonitrile is exothermic by 7.6 kcal·mol^{-1} at the present level of calculation. Therefore, it is not possible to discard that the solvent might have an important role in the reaction path, although we consider that solvent assistance is less likely that the described path from **g** to **h**, which has an energy barrier of only 1.4 kcal·mol^{-1} (Figure 4). The bulky counteranions PF_6^- present in the experimental solution are unlikely to assist a direct proton transfer from **g** to **l** due to sterical reasons.

We have also considered the possibility that, as proposed by Casella and co-workers,[13b] a μ-η^1:η^1-hydroperoxo-Cu^{II}_2 intermediate (see Figure 6) could be an active species in the reaction pathway. However, although protonation of species **d** cannot be ruled out under the experimental conditions used, the orientation of the σ^* orbitals of the hydroperoxo with respect to the HOMO-π orbital of the arene is not appropriate for further reactivity. The macrocyclic constrain of the ligand does not favor a hydroperoxide reacting species, since both aromatic rings are located far from the hydroxyl group.

In the σ^* electrophilic attack mechanism shown in Figures 2 and 4, the $Cu_2O_2^{2+}$ moiety is perpendicular to the attacked aromatic ring plane, as seen in species **e**. We have also analyzed the possible intramolecular π^* electrophilic attack of the $Cu_2O_2^{2+}$ core to the second aromatic ring of the ligand (placed below the peroxo moiety in species **e**, thus bearing a parallel orientation with respect to the $Cu_2O_2^{2+}$ moiety).[5e] However, starting from **e**, an initial rotation of the peroxo group leads to an orientation which is proper for a σ^* attack, and not for a π^* attack, as shown in transition state **TS-em**, to subsequently give species **m** (Figure 7). Species **m** is geometrically and energetically comparable to species **g**. However, **TS-em** is 7.5 kcal·mol^{-1} higher in energy than transition state **TS-ef**, which suggests that the most favored pathway is that shown in Figures 2 and 4. Furthermore, the product for this alternative mechanism is species **n**, which is similar to species **l** of the mechanism shown in Figures 2 and 4. In fact, after some rearrangements of the aromatic rings with no high energetic cost, the two mechanisms corresponding to attack of the $Cu_2O_2^{2+}$ moiety to the two differently orientated aromatic rings converge to the same route. Transition state **TS-nl** of Figure 7 links intermediate

n of this alternative mechanism with product **l** with a barrier of only 6.9 kcal·mol^{-1}. Overall, the geometrical constraints imposed by the macrocyclic ligand preclude a proper orientation for a π* attack.[8c,31,37,38]

Conclusions

In summary, we have reported for the first time a plausible full reaction pathway for the activation of O_2 by a hexaazamacrocyclic dicopper(I) complex (**a**) and for the subsequent intramolecular aromatic hydroxylation to finally yield the μ-phenoxo-μ-hydroxo product (**l**). Despite the lack of experimental spectroscopic evidence to discern between μ-η^2:η^2-peroxo or bis(μ-oxo) species, the present study suggests an energetically favored σ*-mechanism that goes through a μ-η^2:η^2-peroxo species. It is important to stress that, first, the isomeric bis(μ-oxo) species is not far in energy and, second, the relative energies between these two isomers is highly dependent on the method of calculation. For these two reasons, the possibility that the bis(μ-oxo) species is the active species in this reaction mechanism cannot be ruled out. Noteworthy, the key concept highlighted for the first time in this work is that proton release from the attacked C−H bond is assisted by the close presence of another aromatic ring. This strategy allows diminishing energy barriers along the reaction pathway and we envision that this can be a beneficial strategy to design new systems with improved reactivity by the rational design of ligands that place a second aromatic ring in the proper position to assist the deprotonation step. Incidentally, this structural motif may be present in the active site of tyrosinase since histidine moieties close to the tyrosine of the substrate may assist the proton release and promote the reaction.[5g] The lack of high energy barriers and deep energy wells in the studied reaction mechanism explains the difficulty to experimentally trap intermediates within this system (see Figure 8).

Acknowledgment. A. P. thanks the Spanish MEC for a postdoctoral fellowship. Helpful comments from Prof. W. B. Tolman, Dr. M. Costas, Prof. M. C. Holthausen, and Dr. M. Swart are greatly appreciated. We thank financial support from the Spanish MEC (Projects CTQ2005-08797-C02-01/BQU, CTQ2006-05367/BQU, CTQ-2007-67918, CSD2006-0003, and CTQ2008-03077/BQU) and by the Catalan DURSI (project 2005SGR-00238).

Note Added in Proof. During the revision process of this paper, another theoretical paper has appeared reporting mechanistic details on an intramolecular aromatic hydroxylation by a peroxo side-on Cu_2O_2 core (Sander, O. et al. *Chem.−Eur. J.* **2008**, *14*, 9714−9729), as well as a computational work describing the hydroxylation of phenol by the natural tyrosinase enzyme (Inoue, T. et al. *J. Am. Chem. Soc.* **2008**, doi: 10.1021/ja802618s).

Supporting Information Available: Complete computational methods used and xyz coordinates; ChemDraw and full 3D drawings of all stationary points found. Complete ref 18. This material is available free of charge via the Internet at http://pubs.acs.org.

JA801913B

(37) Lam, B. M. T.; Halfen, J. A., Jr.; Hagadorn, J. R.; Holland, P. L.; Lledós, A.; Cucurull-Sánchez, L.; Novoa, J. J.; Álvarez, S.; Tolman, W. B. *Inorg. Chem.* **2000**, *39*, 4059–4072.

(38) (a) Company, A.; Gómez, L.; Mas-Ballesté, R.; Korendovych, I. V.; Ribas, X.; Poater, A.; Parella, T.; Fontrodona, X.; Benet-Buchholz, J.; Solà, M.; Que, L., Jr.; Rybak-Akimova, E. V.; Costas, M. *Inorg. Chem.* **2007**, *46*, 4997–5012. (b) Company, A.; Gómez, L.; Mas-Ballesté, R.; Korendovych, I. V.; Ribas, X.; Poater, A.; Parella, T.; Fontrodona, X.; Benet-Buchholz, J.; Solà, M.; Que, L., Jr.; Rybak-Akimova, E. V.; Costas, M. *Inorg. Chem.* **2006**, *45*, 5239–5241.